Journal of Molecular Structure 1039 (2013) 219–226

Contents lists available at SciVerse ScienceDirect

Journal of Molecular Structure

journal homepage: www.elsevier.com/locate/molstruc

Synthesis and mesomorphism of new chiral imines and copper(II) complexes

Manoj K. Paul [a,*], Gayatri Kalita [a], Atiqur Rahman Laskar [a], Trirup D. Choudhury [b], Nandiraju V.S. Rao [a]

[a] Chemistry Department, Assam University, Silchar 788 011, Assam, India
[b] Department of Chemistry, Karimganj College, Karimganj 788 710, Assam, India

ARTICLE INFO

Article history:
Received 21 July 2012
Received in revised form 14 January 2013
Accepted 6 February 2013
Available online 20 February 2013

Keywords:
Liquid crystals
Chirality
Metallomesogens
Schiff base and copper(II) complexes

ABSTRACT

The synthesis, characterization and mesomorphic properties of a series of N-(2-hydroxy-4-n-alkyloxybenzylidene) 4′-amino-2-methylbutylcinnamate and their copper(II) complexes are reported. The imines exhibited smectic A (SmA) and chiral smectic C (SmC*) phases while their copper(II) complexes displayed SmA–SmC phase variant. The compounds have been characterized by elemental analysis and spectroscopic studies. The phase transition temperatures were detected by differential scanning calorimetry (DSC) analysis and the phases are confirmed by polarizing optical microscopy (POM). The chiral phase (SmC*) of the ligand disappeared on complexation. The unwinding of the helical superstructure of SmC* phase under the influence of electric field and the observed optical textures of SmC* phase are also discussed.

1. Introduction

Materials exhibiting different functional properties can be derived by a combination of organic moieties with soft material properties and metal compounds possessing inherent rich electromagnetic characteristics. Ferroelectric liquid crystals possess unique combination of polar symmetry, spontaneous polarization and fluidity, which make them as potential candidate for modern technological application [1,2]. Meyer et al. [3,4] discovered ferroelectricity in the chiral smectic C (SmC*) phase of liquid crystals derived from molecules possessing chiral center which lift the centro-symmetry of the molecule. Several chiral smectic liquid crystalline compounds showing ferroelectric and anti-ferroelectric [5–7] properties have been synthesized and well studied. The liquid crystals derived from benzylidene cores offer multifaceted advantages, e.g. ease of synthesis, variety of liquid crystalline phases and at ambient temperatures, availability of materials for different experimental investigations as model compounds. The presence of ortho hydroxyl group in benzylidene moiety enhances the stability of imines through intra-molecular hydrogen bonding and contributes to the rigidity and polarizability of the mesogenic nucleus. The introduction of the polar hydroxyl group in a lateral position of the molecule promoted the SmC/SmC* temperature range. For example, the resorcylidene aniline core [8–10] present in calamitic ferroelectric liquid crystals such as in 2-methylbutylresorcylidene aniline (MBRA) and 2-methyloctylresorcylidene aniline (MORA) series exhibits superior mesogenic behavior and more stability towards hydrolysis than benzylidene aniline core because of intramolecular hydrogen bonding. Sakurai et al. reported [11] that the introduction of ortho hydroxyl group to imine linkage in a chiral Schiff base increases the mesomorphic range of chiral SmC* phase. During the last three decades the metallomesogens (metal-containing liquid crystalline molecules) of d- and f-block metals have attracted the attention of several research groups [12–25] because of their unusual geometries, and functional properties viz., ferro-electricity, non-linear optical property, etc. Ferroelectric properties had been realized in Schiff bases viz., [N(4-n-decyloxy salicylidene) 4′-substituted alkyl aniline] when the end alkyl moiety is replaced with a chiral tail [26]. Baena et al. reported [27,28] the first examples of paramagnetic and ferroelectric copper(II) and vanadium(IV) complexes (Fig. 1) of chiral Schiff bases. Wide thermal range of SmC* phase is realized in copper(II), vanadium(IV) and palladium(II) complexes [29] of lateral-lateral fused twin ferroelectric metal–organic liquid crystals. Recently, a new class of low molar mass chiral metallomesogens containing cholesterol based N-(n-alkyl)salicylideneimines displayed chiral nematic (N*) and smectic A (SmA*) phases [30]. In this paper, we report the synthesis, spectroscopic characterization, photo-physical and mesomorphic properties of a new series of copper(II) complexes derived from chiral imines.

2. Experimental

2.1. Physical measurements

UV–Visible absorption spectra of the compounds in $CHCl_3$ were recorded on a Shimadzu UV-1601PC spectrophotometer. Infrared spectra were recorded on a Perkin Elmer L 120-000A spectrometer using a KBr disk. The ^1H NMR spectra were recorded on a Bruker

* Corresponding author. Tel.: +91 3842270848.
E-mail address: paulmanojaus@gmail.com (M.K. Paul).

0022-2860/$ - see front matter © 2013 Elsevier B.V. All rights reserved.
http://dx.doi.org/10.1016/j.molstruc.2013.02.007

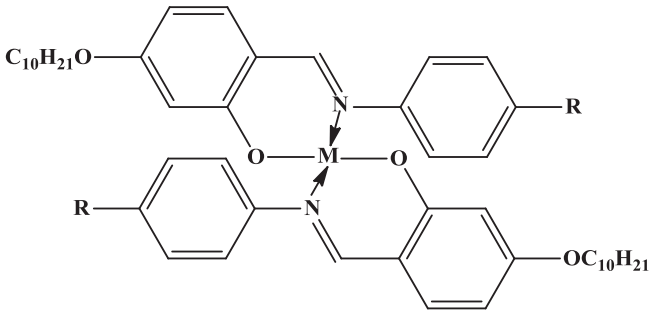

R = -CH=CHCOOC*H(CH$_3$)COO(CH$_2$)$_2$CH$_3$
and -CH=CH-COO-C*H(CH$_3$)COOC$_4$H$_9$
M = Cu(II) and VO(IV)

Fig. 1. Molecular structure of the paramagnetic Schiff base complexes reported [27,28].

DPX400 MHz spectrometer in $CDCl_3$ (chemical shift in δ) solution with TMS as internal standard. Molar conductance of a representative ligand and its complex were determined in dimethylformamide (ca. 10^{-3} mol L^{-1}) at room temperature using Systronics CM304 conductivity meter. The optical textures to characterize the different mesophases of the compounds were observed using a polarizing microscope (Nikon Optiphot2pol), equipped with hot stage (Instec hot- and cold-stage HCS302 with STC200 temperature controller). The accuracy in temperature measurement is ±0.1 °C. The phase transition temperatures and associated enthalpies of the compounds were recorded using differential scanning calorimeter (DSC Perkin–Elmer Pyris1 system) at a heating or cooling rate of 5 °C min^{-1}. The electric field experiments were performed using 20 Mz function generator (33220A Agilent). The optical studies on free standing film were studied by an indigenously assembled depolarized reflected light microscopy (DRLM).

2.2. Materials

The organic reagents required for the synthesis of chiral imines and their copper(II) complexes were procured from Tokyo Kasei (Japan), E. Merck (Germany), Aldrich (USA), BDH (India), Frinton Chemicals (USA), Eastman Kodak Company (USA) and have been used without further purification. The solvents used (viz. ethanol, chloroform, n-hexane) are purified by the standard procedures well documented in literature. Silica (60–120 mesh) from Spectrochem was used for chromatographic separation and silica gel G (E. Merck, India) for TLC.

The synthetic routes used for the preparation of chiral imines and their mononuclear Cu(II) complexes:

The synthesis of the materials was carried out following the procedures well documented in literature with little modification [31–34]. The synthetic route for the preparation of imines and mono nuclear copper(II) complexes are shown in Scheme 1.

2.3. Synthesis of 4-n-alkyloxysalicyldehyde (*1*)

4-n-Alkyloxysalicylaldehydes (**1a**–**i**) were synthesized and purified following the procedures described previously [32–34]. All the compounds are obtained in good yield.

2.4. Synthesis of N-(4-n-pentyloxy-2-hydroxybenzylidene)-2-methylbutyl-4′-aminocinnamate (*2a*)

All the chiral ligands were synthesized by condensing appropriate 4-n-alkoxy salicylaldehyde with (+)-2-methylbutyl-4-amino cinnamate in an ethanolic solution. About 200 mg (1 mmol) of 4-n-pentyloxysalicylaldehyde dissolved in hot ethanol and an equimolar ethanolic solution of (+)-2-methylbutyl-4-amino cinnamate (230 mg, 1 mmol) added drop wise with a few drops of glacial acetic acid as catalyst and refluxed for 3 h to yield the yellow Schiff base. The precipitate was collected by filtration and recrystallized several times from absolute ethanol to give a pure compound. Yield = 260 mg (61%).

IR (ν_{max}, cm^{-1}, KBr): 3442 (ν_{OH}, H bonded), 2925($\nu_{as\ (C-H)}$ CH_3 and CH_2) and 2855($\nu_{s\ (C-H)}$ CH_3 and CH2), 1702 ($\nu_{C=O}$, ester), 1629 ($\nu_{C=N}$, imine), 1241 (ν_{C-O}).

^{1}H NMR (300 MHz, $CDCl_3$): δ = 13.54 (s, 1H, O**H**), 8.54 (s, 1H, C**H**=N), 7.68 (d, 1H, *J* = 16.2 Hz, —C=C**H**—, α proton), 7.57–6.48 (m, 7H, Ar—**H**), 6.44 (d, 1H, *J* = 16.2 Hz, —C=C**H**—, β proton), 4.24 (t, *J*=C**H**$_2$—COO—), 4.11 (s, 1H, tertiary C—**H**), 4.00 (t, *J* = 6.9 Hz, —OC**H**$_2$—), 1.78–1.17 (m, 10H, —(C**H**$_2$)—), 0.97 (t, 9H, *J* = 6.6 Hz, C**H**$_3$). ^{13}C NMR ($CDCl_3$): δ = 11.4, 14.1, 16.6, 22.7, 25.8, 26.3, 29.0, 29.1, 31.7, 34.4, 68.8, 69.4, 101.2, 102.0, 108.9, 115.8, 118.4, 121.6, 129.5, 130.0, 134.5, 135.4, 143.6, 164.7, 167.9, 178.6. Analysis Calc. for $C_{26}H_{33}NO_4$: C, 73.73; H, 7.85; N, 3.31. Found: C, 73.56; H, 7.53; N, 3.01.

All the homologues (**2a**–**2i**) were synthesized following the same procedure. The FTIR, ^{1}H NMR and CHN data of Schiff bases (**2a**–**2i**) are presented in ESI **1E**.

2.5. Synthesis of Bis[N-(4-n-hexyloxysalicylidene)-2-methylbutyl-4′-aminocinnamate]-copper(II) complex (*3a*)

The ligand N-(4-n-pentyloxy-2-hydroxybenzylidene)-2-methylbutyl-4′-aminocinnamate (840 mg, 2 mmol) was dissolved in minimum volume of absolute ethanol and refluxed for 30 min. To this refluxing solution an ethanolic solution containing copper acetate monohydrate $Cu(CH_3COO)_2{\cdot}H_2O$ (200 mg, 1 mmol) was added drop wise and refluxed it for another 3 h. The color of the solution changed from yellow to brown. The brown precipitate appeared on cooling to room temperature was filtered off and washed with ethanol and then repeatedly recrystallized from chloroform/ethanol (1:3). Yield = 289 mg (61%).

IR (ν_{max}, cm^{-1}, KBr): 2959($\nu_{as\ C-H}$ for CH_3 and CH_2) and 2853($\nu_{s\ C-H}$ for CH_3 and CH_2), 1711 ($\nu_{C=O}$, ester), 1610 ($\nu_{C=N}$, imine), 1141 (ν_{C-O}).

Experimental analysis. Calc. for $C_{52}H_{64}CuN_2O_8$: C, 68.74; H, 7.10; N, 3.08. Found C, 68.70; H, 7.05; N, 3.01.

Similar procedure was adopted for the preparation of other complexes (**3b**–**i**). The FTIR CHN data of Cu(II) complexes (**3a–3i**) are presented in ESI **2E**.

3. Results and discussion

The composition of chiral imines (**2a**–**i**) and corresponding Cu(II) complexes (**3a**–**i**) were confirmed by elemental analysis. The molecular structures were characterized by various spectroscopic methods, e.g. FTIR, ^{1}H NMR and UV–Visible spectra. The spectroscopic data confirmed the proposed molecular structures. The liquid crystalline property was established by polarizing microscopy and DSC study. The optical studies on free standing film experiment were performed in one of the compound **2c** under electric field. The electric field study was carried out on a thin film of chiral ligand **2a** to investigate the effect of the electric field on helicity.

3.1. FTIR Study

The IR spectra of the ligands (**2a–i)** showed the —CH=N— stretching at the expected values of ~1627 cm^{-1}, which has been shifted to a lower frequency by ca. 10–12 cm^{-1} as compared to that

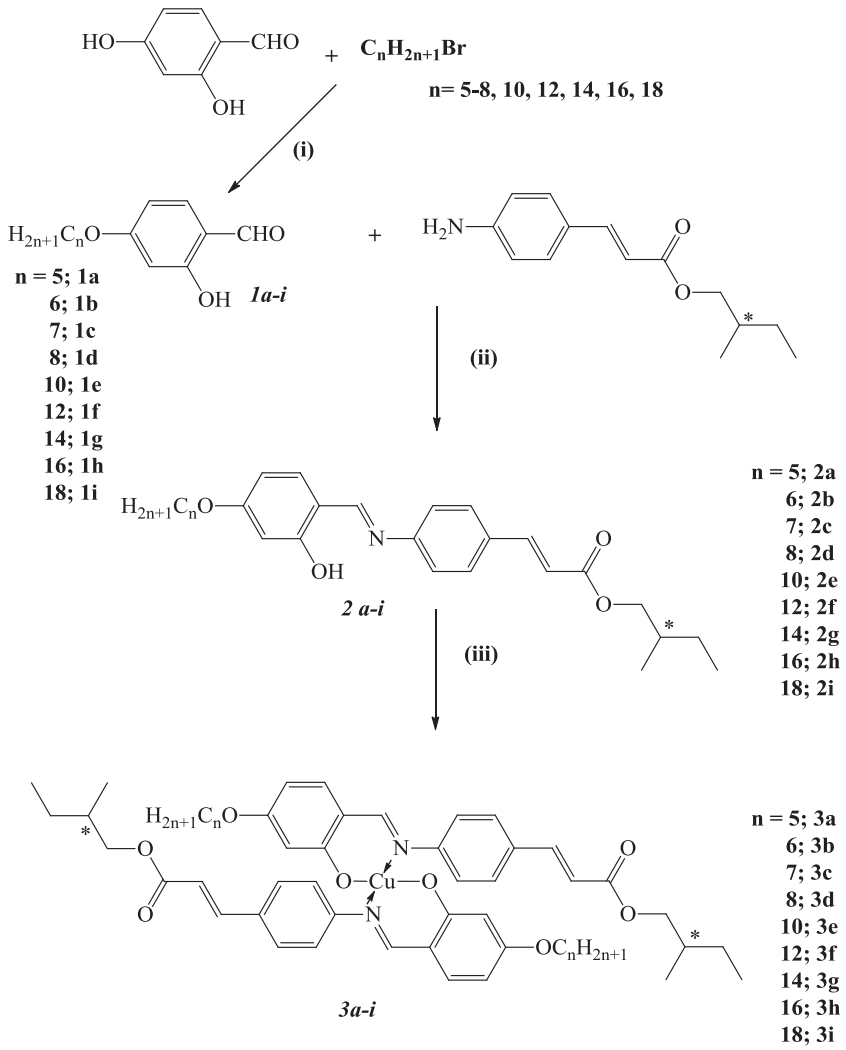

Scheme 1. The synthetic route for the preparation of chiral imines and its mono nuclear copper(II) complexes. Reagent and conditions: (i) $KHCO_3$, dry acetone, KI (catalytic amount), reflux for 24 h; (ii) Absolute ethanol, glacial acetic acid (2–3 drops), reflux for 3 h; (iii) $Cu(CH_3COO)_2{\cdot}H_2O$, ethanol, reflux for 4 h.

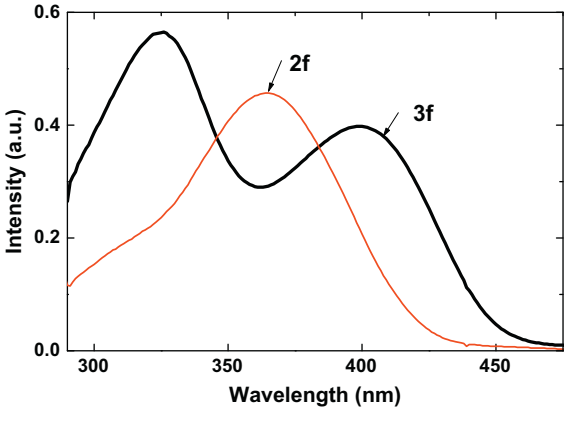

Fig. 2. UV–Visible absorption spectrum of chiral Schiff base ligand (**2f**) and Cu(II) complex (3f) recorded in chloroform at same concentration ($c = 10^{-5}$ mol L^{-1}).

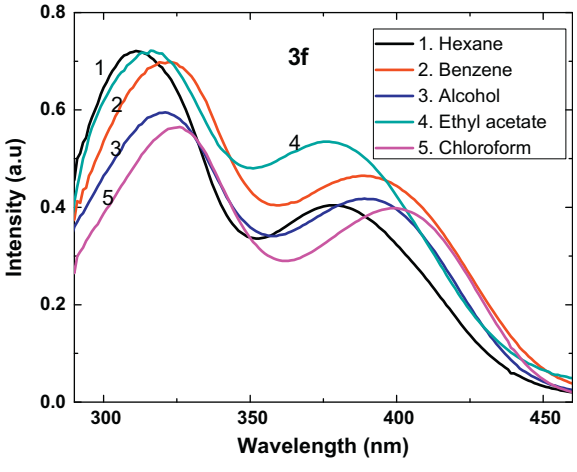

Fig. 3. UV–Visible absorption spectrum of Cu(II) complex (3f) recorded in various solvent at same concentration ($c = 10^{-5}$ mol L^{-1}).

of the free imine upon complexation with copper(II). This shift in frequency confirmed the formation of Cu(II) complexes [35,36]. The stretching band of the C=C bond of cinnamate moieties of imine ligands remain unchanged after complexation with the metal ion. The observed stretching band at 1702–1710 cm^{-1} region was assigned to ester group (—COO—) of cinnamate moieties of the ligands (**2a–i**) and complexes (**3a–i**). The C—O stretching

Table 1
Mesomorphic phase transition temperatures (T °C), associated enthalpies (ΔH *italics*, kJ mol^{-1}) and entropy (ΔS *in italics* J mol^{-1} K^{-1}) for the chiral imines (**2a–2f**) are presented in parenthesis.

Chiral imines	Heating cycle				Cooling cycle			
	Cr	SmC*	SmA	Iso	Iso	SmA	SmC*	Cr
2a	• 78.6 *[17.9, 50.9]*	• 105.4^{tm}	• 144.7 *[4.8, 11.4]*	•	• 143.3 *[4.7, 11.3]*	• 104.8 ^{tm}	• 59.1 *[15.6, 46.9]*	•
2b	• 94.9 *[22.3, 60.4]*	• 109.6 ^{tm}	• 143.5 *[4.4, 10.3]*	•	• 143.0 *[3.8, 8.9]*	• 104.2 ^{tm}	• 82.3 *[20.1, 56.6]*	•
2c	• 94.9 *[23.7, 64.6]*	–	• 142.9 *[4.7, 11.3]*	•	• 142.1 *[4.4, 10.4]*	• 82.2 *[22.3, 62.9]*	–	•
2d	• 95.2 *[24.7, 67.2]*	• 117.0 *[0.02, 0.05]*	• 141.8 *[5.4, 12.7]*	•	• 141.3 *[5.3, 12.5]*	• 115.9 *[0.17, 0.44]*	• 66.4 *[16.3, 18.2]*	•
2e	• 88.5 *[21.8, 60.3]*	• 113.8 *[0.03, 0.09]*	• 140.6 *[5.5, 13.0]*	•	• 140.3 *[5.4, 13.0]*	• 112.9 *[0.16, 0.42]*	• 65.3 *[20.2, 59.7]*	•
2f	• 77.2 *[19.2, 50.9]*	• 95.5 ^{tm}	• 139.3 *[5.7, 13.7]*	•	• 139.0 *[5.5, 13.2]*	• 80.1 ^{tm}	• 59.1 *[19.4, 58.5]*	•
2g	• 76.2 *[21.1, 60.4]*	• 83.6 ^{tm}	• 138.6 *[4.7, 11.4]*	•	• 137.4 *[3.8, 9.2]*	• 75.5 ^{tm}	• 54.9 *[17.4, 52.9]*	•
2h	• 67.0 *[46.7, 137.5]*	• 101.5 ^{tm}	• 137.5 *[5.9, 14.3]*	•	• 136.4 *[5.6, 13.6]*	• 89.3 ^{tm}	• 53.2 *[32.0, 98.1]*	•
2i	• 68.1 *[43.5, 127.5]*	-	• 128.8 *[2.5, 6.3]*	•	• 126.7 *[3.2, 8.0]*	• 56.7 ^{tm}	• 55.8 *[47.8, 145.3]*	•

^{tm} Indicates POM observed values. Here, Cr = Crystalline phase, SmA = smectic A phase, SmC* = chiral smectic C phase. Heating and cooling rates are 5 °C min^{-1} for the melting and clearing processes.

Table 2
Mesomorphic phase transition temperatures (T °C), associated enthalpies (ΔH *in italics* kJ mol^{-1}) and entropy (ΔS *in italics* J mol^{-1} K^{-1}) for Copper(II) complexes are presented in parenthesis.

Complexes	Heating cycle				Cooling cycle			
	Cr	SmC	SmA	Iso	Iso	SmA	SmC	Cr
3a	• 145.8 *[24.7, 59.1]*	• 160.9 *[0.11, 0.26]*	• 199.5 *[6.8, 14.5]*	•	• 196.7 *[6.9, 14.7]*	• 156.9 *[0.15, 0.35]*	• 117.5 *[20.9, 53.6]*	•
3d	• 141.1 *[21.0, 50.8]*	• 165.6^{tm}	• 193.8 *[6.8, 14.6]*	•	• 187.8 *[4.1, 9.0]*	• 160.4^{tm}	• 111.6 *[4.0, 10.1]*	•
3e	• 163.6 *[36.5, 83.4]*	• 170.7 *[0.08, 0.18]*	• 203.9 *[7.6, 16.0]*	•	• 199.3 *[5.4, 11.5]*	• 162.8 *[0.18, 0.42]*	• 123.7 *[13.0, 32.8]*	•
3f	• 145.8 *[145.8, 26.1]*	• 139.7 ^{tm}	• 198.6 *[7.3, 15.4]*	•	• 196.6 *[7.2, 15.4]*	• 132.2 ^{tm}	• 117.1 *[24.0, 61.7]*	•
3g	• 141.3 *[26.1, 63.0]*	• 151.9 *[0.11, 0.27]*	• 194.3 *[8.0, 17.2]*	•	• 188.1 *[6.1, 13.3]*	• 141.7 *[0.21, 0.52]*	• 107.8 *[21.6, 56.7]*	•
3h	• 129.1 *[11.0, 27.3]*	• 176.9 ^{tm}	• 182.3 *[7.4, 16.3]*	•	• 179.7 *[7.5, 16.6]*	• 174.6 ^{tm}	• 100.1 *[16.9, 45.4]*	•
3i	• 135.2 *[23.9, 58.6]*	–	• 183.7 *[7.5, 16.5]*	•	• 182.6 *[2.1, 4.7]*	• 181.5 *[2.4, 5.3]*	• 110.4 *[22.7, 59.3]*	•

^{tm} Indicates POM observed values. Here, Cr = Crystalline phase, SmA = smectic A phase, SmC = smectic C phase. Heating and cooling rates are 5 °C min^{-1} for the melting and clearing processes.

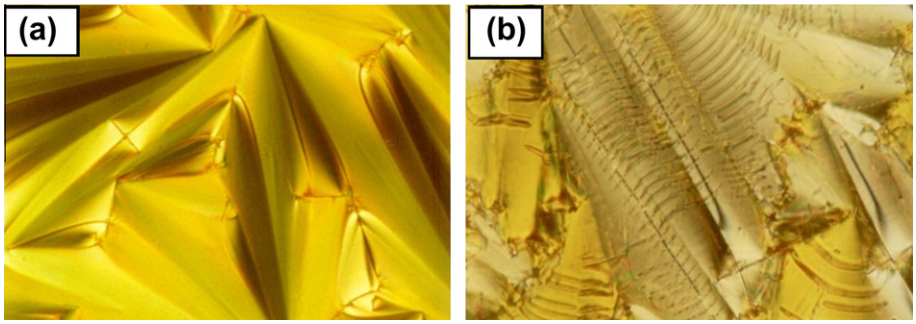

Fig. 4. (a) Focal conic fan texture of the SmA phase of **2a** at 140.5 °C on the cooling the sample and (b) equidistant chiral lines running across fan-shaped texture of SmC* phase at 104.7 °C during phase transition of **2a**.

frequency which appeared at ~1242 cm^{-1} for the imine ligands (**2a–i**) is shifted to lower frequency ~1142 cm^{-1} for the complexes (**3a–i**) indicating the coordination of the metal through phenolic oxygen.

3.2. ^{1}H NMR Study

The ^{1}H NMR data was found to be in good agreement with the proposed structures of the ligand. ^{1}H NMR spectra of the ligands (**2a–2i**) show a signal at δ = 13.4–13.8 ppm, corresponding to the proton of the hydroxyl (—OH) group. The imine proton appeared at δ = 8.50 ppm for ligands and confirmed the formation of the Schiff base [35,36]. All other aromatic protons appeared in the range of δ = 7.57–6.48 ppm. The two protons of the C=C of the cinnamate appeared at δ = 7.68 and 6.44. The proton attached to the chiral carbon appeared as a singlet at δ = 4.11 ppm. The NMR spectra of the complexes are not recorded because of paramagnetic nature of the Cu(II) atom.

3.3. Optical absorption studies

The UV–Visible spectra of both chiral imines and its mononuclear copper(II) complexes are recorded in chloroform at concentration 1×10^{-5} mol L^{-1} (chloroform was chosen because of maximum solubility of the compounds). The UV-spectra of the ligands exhibited (Fig. 2) a characteristic absorption of —CH=N— bond at 364 nm (ε = 46,700 L mol^{-1} cm^{-1}) due to π–π^* transitions of imine linkage. This band shifted (~39 nm) towards higher energy region upon complexation and appeared at 325 nm (ε = 56,400 L mol^{-1} cm^{-1}) in copper(II) complexes. For copper(II) complexes another broad peak appeared at lower energy region 401 nm (ε = 39,700 L mol^{-1} cm^{-1}), and corresponds to ligand to metal or metal to ligand charge transfer. Solvatochromic effect was also observed in copper(II) complexes; the absorption maxima of both π–π^* band and charge transfer band shifted on changing the polarity of the solvent. The shift in absorption maxima occurred in an irregular manner, with a change in polarity of the

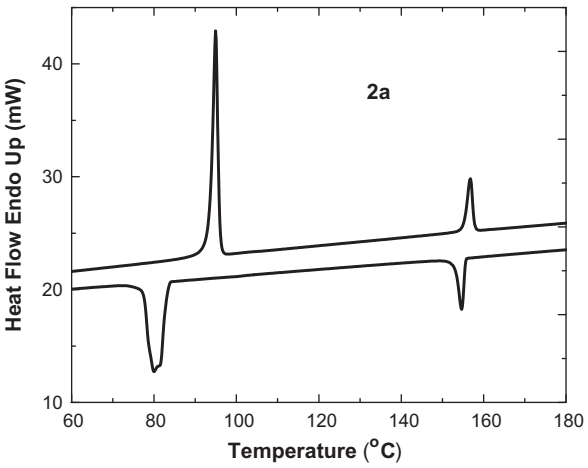

Fig. 5. Representative DSC thermogram of ligand **2a** in the second heating and cooling cycles at 5 °C/min.

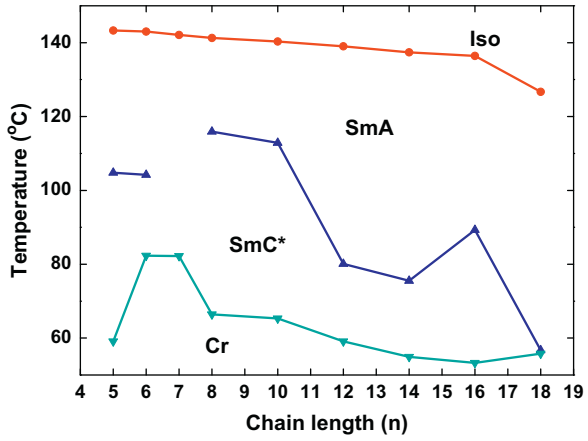

Fig. 6. Variation of phase transition temperatures as a function of alkyl chain length (n) of chiral imines.

solvent (Fig. 3). However no such effect was observed in the chiral ligand. Solvatochromism is usually indicative of nonlinear optical (NLO) property of the compound and it arises due to changes in dipole moments ($\Delta\mu$) between the ground and excited states upon excitation in complexes.

3.4. Conductivity measurements

The molar conductance of a representative ligand (**2f**) and copper complex (**3f**) in dimethylformamide were found to be 1.9 and 1.4 Ω^{-1} cm^2 mol^{-1} respectively. The conductance values are very low compared to 1:1 electrolyte [37], which indicates that the chiral imine and the metal complexes are not ionized in solution. The low conductivity values infer that imine and complex are considered to be neutral and non-electrolytic in nature.

3.5. Thermal microscopy and differential scanning calorimetric studies: mesomorphic behavior

3.5.1. Ligands

The phase transition temperatures and associated enthalpies of chiral imines and copper(II) complexes are summarized in Tables 1 and 2 respectively.

All the chiral imines exhibit enantiotropic chiral smectic C (SmC*) and smectic A (SmA) phases with the lone exception **2c**. On slow cooling the samples, small batonnets grows from isotropic (Iso) melt which developed to a focal conic fan texture of SmA phase as shown in Fig. 4a. The Iso-SmA transition was detected in DSC for **2a** at 143.3 °C with an enthalpy change of 4.74 kJ mol^{-1}. On further cooling arcs appeared on focal conic fan texture of SmA with a typical helical stripe, characteristic of chiral SmC* (Fig. 4b). The SmA–SmC* transition was not detected by DSC only in some samples. The SmC* transformed to crystalline solid on further cooling, and this transition was detected by DSC for **2a** at 59.1 °C with an enthalpy change of 15.59 kJ mol^{-1}. The representative, DSC thermograms of **2a** in the second heating and cooling cycles of chiral ligand recorded at a rate of 5 °C min^{-1} is shown in Fig. 5.

The clearing temperature of the ligands gradually decreases with the increasing chain length. The mesomorphic SmC* phase range do not follow any systematic change as a function of chain length. The phase transition temperatures as a function of chain length is presented in Fig. 6. The appearance of the equidistant line pattern which is a measure of pitch length of SmC* phase and reflects the helical superstructure. The lines are parallel to the smectic layer planes and the distance between two adjacent dark lines gives the pitch of the helix. The helix axis is perpendicular to the lines. But the helical line disappeared when the thickness of the film decreased. This was clearly observed when the sample was melted in a ITO coated cell (thickness 5 μm) treated for homogeneous alignment (Fig. 7). This indicates the unwinding of the helix. In a thin cell, the SmC* phase have book-shelf structure of layers [38]. The unwinding of the helix is driven by the competition between anchoring forces and the natural twisting tendency of the molecules. This competition gives rise to an unwinding transition if the cell thickness is below a critical threshold roughly equal to the helical pitch [5]. Therefore, it is difficult to observe helical lines in the SmC* phase of a planar aligned cell with a thickness of 5 μm. Moreover, the helical lines are distinctly observed when sandwiched in untreated glass plate and coverslip because the surface interactions remain relatively weak and the helical structure is preserved.

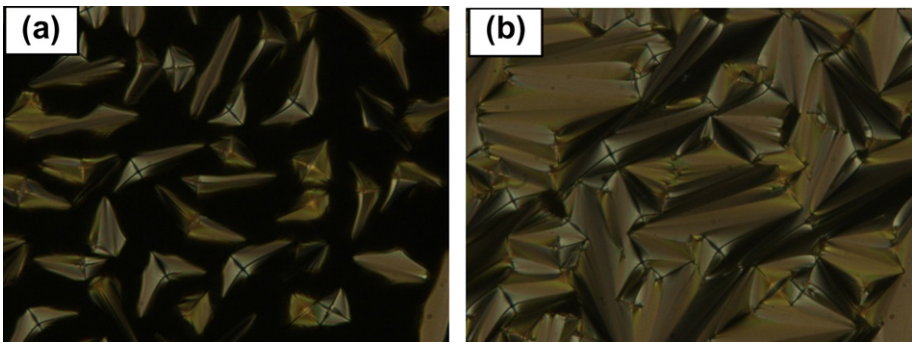

Fig. 7. (a) Batonnets texture of the SmA phase at 147.5 °C and (b) smooth focal conic fan shaped texture at 98 °C of **2a** in planar aligned ITO coated cell of thickness 5 μm.

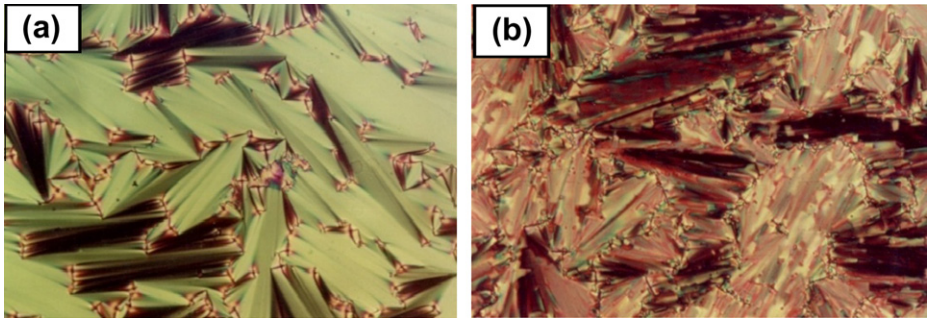

Fig. 8. (a) Focal conic fan texture of the SmA phase of **3a** at 192 °C on the cooling the sample from isotropic phase and (b) broken fan-shaped texture of SmC phase at 152 °C.

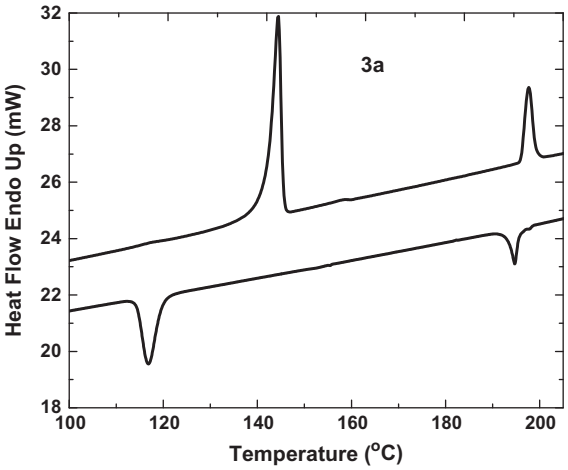

Fig. 9. Representative DSC thermogram of copper(II) complex **3a** in the second heating and cooling cycles at 5 °C/min.

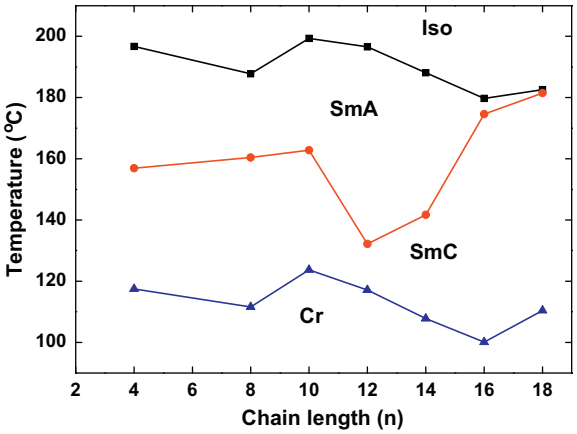

Fig. 10. Variation of phase transition temperatures as a function of alkyl chain length (n) of Cu(II) complexes.

3.5.2. Complexes

All the copper(II) complexes (**3a–i**) exhibit enantiotropic mesomorphism of SmA and SmC phases. The compounds (**3a–i**) are microcrystalline solids at room temperature and upon heating and/or cooling from the isotropic liquid, display smectic mesophase. The enthalpies associated with the transitions are depicted in Table 2. The mesophases shown by the complexes were identified by polarizing microscopy as SmA and SmC by their optical textures as shown in Fig. 8a and b. DSC thermogram of complex 3a (5 °C min^{-1}) is shown in Fig. 9, which are in agreement with the phase transitions observed by POM. We did not observe any helical optical texture in SmC phase of any complex indicating the disappearance of chiral phases exhibited by the ligands. The coordination of the metal ion with the ligand leads to a rigid molecular structure. In the rigid molecular structure the molecular director in axial direction cannot rotate across the layer plane. The broken focal conic fan texture appears on cooling with the absence of stripes confirmed SmC phase [39]. Similar observations of suppression of chirality upon complexation is reported in Cu(II) complexes of chiral cholesterol based dimesogenic ligands [40]. We still do not know any special reasons for the suppression of chirality upon complexation only in some compounds and not in some other compounds [30]. Further work is to be carried out to ascertain the reasons for such suppression of chiral phases upon complexation. The clearing and melting temperatures of the complexes (**3a–i**) are significantly higher than corresponding chiral imines (**2a–i**). It indicated higher thermal stability of the complexes compared to ligands. The phase diagram as function of chain length is presented in Fig. 10. The SmA and SmC phase ranges did not follow any systematic change as a function of chain length. The compounds with longer chain length (**3h** and **3i**) exhibited wide range of SmC phase.

3.6. Electric field study

The helical superstructure of the SmC* phase can be unwound or distorted under the influence of external electric field which derives the reorientation of the molecular long axis along the field direction [41]. The helical structure of SmC* phase linearly distorts and the helical pitch increases, this process is called the distorted-helix ferroelectric effect [42]. If the electric field is increased above a critical threshold, the transition from a helical SmC* to the homogeneous structure SmC occurs, the helical pitch diverges and the helix is unwounded [43–45]. Preliminary investigations of electric field influence on the molecular alignment and helical structure was carried out using a polyimide coated (PI) cell of ~100 μm and applying the electric field of 0–100 V at 50 Hz. The helical pitch unwinding and the reorientation of the molecules with the direction of the electric field or switching phenomena is observed in (**2a**) in SmC* phase. The observed photographs illustrating the switching phenomena, i.e. reorientation of molecules under the influence of electric field (V = 0–100 V, thickness = 100 μm), at 50 Hz are presented (see Fig. 11). The helical structures of SmC* phase when unwound, the equidistant arced lines across the fans disappeared with the increase in the strength of electric field.

3.7. Free standing film

A free standing film of the ligand (**2c**) was prepared in a temperature regulated two stage oven filled with argon at

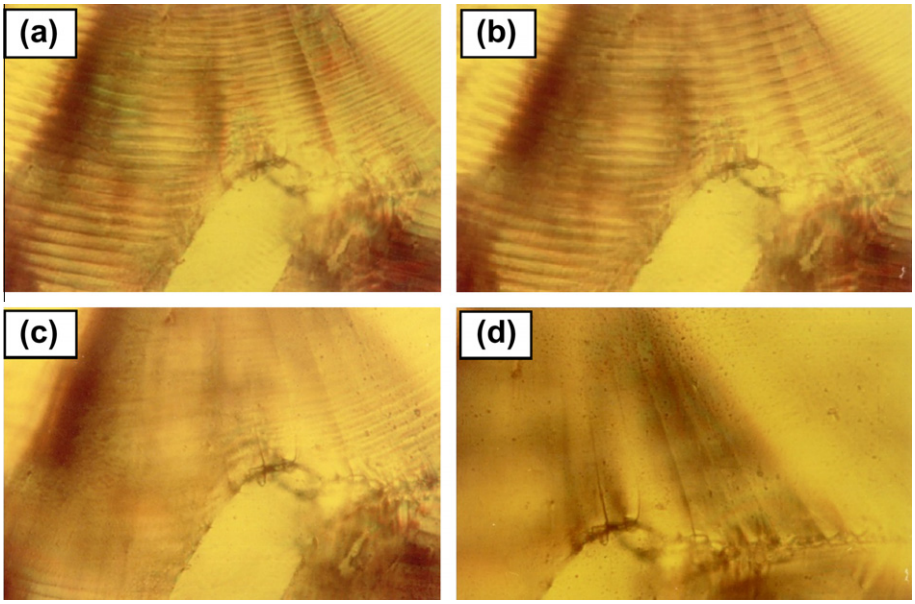

Fig. 11. Changes in optical texture (40×) of **2a** in SmC* phase at 104 °C as a function of electric field, in a PI coated cell thickness ~ 100 μm (a) fan-shaped texture with equidistant lines of SmC* phase at 0 V; (b) increasing distance between striations reflecting the changes in pitch at 10 V; (c) 20 V and (d) the helical super structure completely unwound at 100 V.

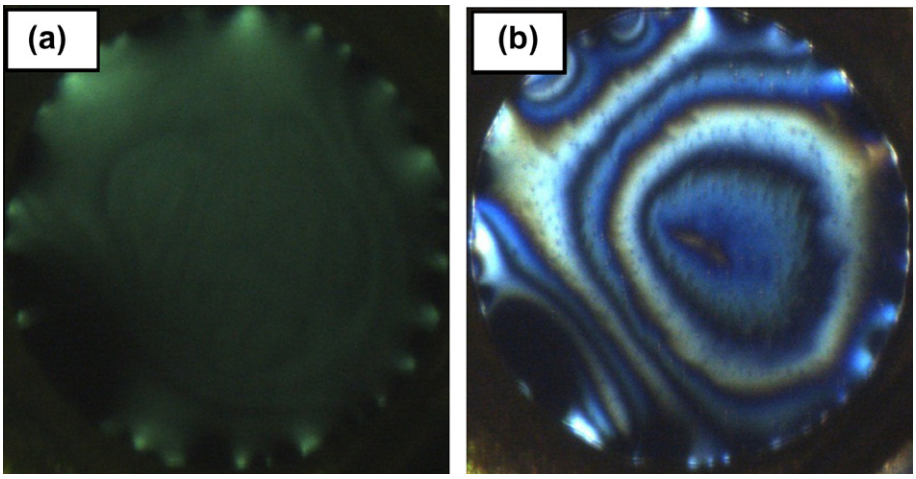

Fig. 12. Optical textures of the free standing film of the ligand **2c** under uncrossed polarizer(~5°): (a) SmA phase at 122 °C; (b) SmC* phase at 94.5 °C.

0.7 atm to minimize the sample degradation. The films were pulled across a circular hole (4 mm diameter) in the center of a glass cover slip in the smectic A phase (T = 147 °C) of the ligand (**2c**). Two electrodes of 5 mm in length were placed on the bottom side of the cover slip and on the opposite side of the hole. The DRLM technique was used to study the optical texture of the free standing film. It was observed that the defect lines (2π wall) appears on the film and moves on the surface of the film. The 2π wall originates due to fact that the c-director rotates in different direction with electric field [46]. The optical texture of the freestanding film in SmA and SmC* phase is presented in Fig. 12. The film responses with electric field when it reached to a chiral SmC* regime indicated by switching phenomenon confirms the ferroelectric phase.

4. Conclusions

The homologous series of chiral imines, N-(4-*n*-alkyloxy-2-hydroxybenzylidene)-2-methylbutyl-4′-aminocinnamates (**2a**–**i**) and their Cu(II) complexes (**3a**–**i**) had been synthesized and characterized. The copper(II) complexes exhibited Solvatochromism indicating them as NLO active materials. The molar conductivity studies confirmed the non-ionic nature of these compounds. The ligand (**2a**–**i**) exhibits enantiotropic SmA–SmC* phase variants. Copper(II) complexes (**3a**–**i**) display enantiotropic SmA–SmC phase variant with an increased thermal stability than the corresponding ligands. The metal complexation of a chiral ligand suppresses the chiral phase and further work is in progress to ascertain the reasons for such behavior.

Acknowledgements

Authors acknowledge Department of Science and Technology, New Delhi for financial assistance and C.C. Huang, School of Physics and Astronomy, University of Minnesota for providing DRLM instrumental facility.

References

[1] S.T. Langerwall, Ferroelectric and Antiferoelectric Liquid Crystals, Wiley VCH, 1999.

[2] H.S. Kitzerow, C. Bahr (Eds.), Chirality in Liquid Crystals, Springer Verlag Inc., New York, 2001.
[3] R.B. Meyer, Mol. Cryst. Liq. Cryst. 40 (1977) 33.
[4] R.B. Meyer, L. Liebert, L. Strzelecki, P. Keller, J. Phys. 36 (1975) L-69.
[5] N.A. Clark, S.T. Lagerwall, Appl. Phys. Lett. 36 (1980) 899.
[6] J.W. Goodby, Ferroelectric Liquid Crystals, Gordon and Breach, Philadelphia, 1991.
[7] A. Fukuda, Y. Takanashi, T. Isozaki, K. Ishikawa, H. Takezoe, J. Mater. Chem. 4 (1994) 997.
[8] B.I. Ostrovskii, A.Z. Rabinovich, A.S. Sonin, E.L. Sorkin, B.A. Strukov, S.A. Taraskin, Ferroelectrics 24 (1980) 309.
[9] A. Hallsby, M. Nilsson, B. Otterholm, Mol. Cryst. Liq. Cryst. 82 (1982) 61.
[10] B. Otterholm, M. Nilsson, S.T. Lagerwall, K. Skarp, Liq. Cryst. 2 (1987) 757.
[11] T. Sakurai, K. Sakamoto, M. Hanma, K. Yossino, M. Ozaki, Ferroelectrics 58 (1984) 21.
[12] J.L. Serrano (Eds.), Metallomesogens, Synthesis, Properties and Applications. VCH, Weinheim, Germany, 1996.
[13] A.M. Giroud-Godquin, Metal containing Liquid Crystals, in: D. Demus, J.W. Goodby, G.W. Gray, H.W. Spiess, V. Vill (Eds.), Handbook of Liquid Crystals, vol. IIB, Wiley-VCH, Weinheim, Germany, 1998.
[14] A.M. Giroud-Godquin, P.M. Maitlis, Angew. Chem. Int. Ed. Engl. 30 (1991) 375.
[15] P. Espinet, M.A. Esteruelas, L.A. Oro, J.L. Serrano, E. Sola, Chem. Rev. 117 (1992) 215.
[16] D.W. Bruce, in: D.W. Bruce, D. O'Hare (Eds.), Inorganic Materials, second ed., Wiley, Chichester, 1996, pp. 405–490 (Chapter 8).
[17] D.W. Bruce, J. Chem. Soc., Dalton Trans. (1993) 2983.
[18] A.P. Polishchuk, T.V. Timofeeva, Russ. Chem. Rev. 62 (1993) 291.
[19] S.A. Hudson, P.M. Maitlis, Chem. Rev. 93 (1993) 861.
[20] L. Oriol, J.L. Serrano, Adv. Mater. 7 (1995) 348.
[21] N. Hoshino, Chem. Rev. 174 (1998) 77.
[22] B. Donnio, D.W. Bruce, Struct. Bond. 95 (1999) 193.
[23] B. Donnio, D. Guillon, R. Deschenaux, D.W. Bruce, in: J.A. McCleverty, T.J. Meyer (Eds.), Comprehensive Coordination Chemistry II: From Biology to Nanotechnology, vol. 7, Elsevier, Oxford, UK, 2003, pp. 357–627.
[24] D.W. Bruce, R. Deschenaux, B. Donnio, D. Guillon, in: R.H. Crabtree, D.M.P. Mingos (Eds.), Comprehensive Organometallic Chemistry III, vol. 12, Elsevier, Oxford, UK, 2007, pp. 195–293 (Chapter 12.05).
[25] P. Espinet, J. Etxebarria, M. Marcos, M.A. Perez-Jubindo, M.B. Ros, J.L. Serrano, Mater. Res. Soc. Symp. Proc. 392 (1995) 123.
[26] M. Guillevic, M.J. Danks, S.K. Harries, S.R. Collinson, A.D. Pidwell, D.W. Bruce, Polyhedron 19 (2000) 249.
[27] M.J. Baena, P. Espinet, M.B. Ros, J.L. Serrano, A. Ezcurra, Angew. Chem. Int. Ed. Engl. 32 (1993) 1203.
[28] M.J. Baena, J. Barbera, P. Espinet, A. Ezcurra, M.B. Ros, J.L. Serrano, J. Am. Chem. Soc. 116 (1994) 1899.
[29] R. Iglesias, M. Marcos, J.L. Serrano, T. Sierra, Chem. Mater. 8 (1996) 2611.
[30] G. Shanker, C.V. Yelamaggad, J. Mater. Chem. 21 (2011) 15279.
[31] C.K. Lai, Y. Leu, Liq. Cryst. 25 (1998) 689.
[32] N.V.S. Rao, T.D. Choudhury, M.K. Paul, T. Francis, Liq. Cryst. 36 (Suppl.) (2009) 409.
[33] P. Keller, L. Liebert, Solid State Phys. 14 (1978) 19.
[34] M. Artigas, M. Marcos, E. Melendez, J.L. Serrano, Mol. Cryst. Liq. Cryst. 130 (1985) 337.
[35] F.R. Diaz, N. Valdebenito, J.L. Serrano, M. Marcos, J.I. Martinez, P.J. Alonso, Liq. Cryst. 25 (1998) 217.
[36] M. Ghedini, S. Morrone, D. Gatteschi, C. Zanchini, Chem. Mater. 3 (1991) 752.
[37] W.J. Geary, Coord. Chem. Rev. 7 (1971) 81.
[38] A.D. Rey, Phys. Rev. E 53 (1996) 4198.
[39] I. Dierking, Texture of Liquid Crystals, Wiley-VCH Verlag GmbH and Co. KGaA, Weinheim, 2003 (Chapter 7).
[40] C.V. Yelamaggad, U.S. Hiremath, D.S.S. Rao, Liq. Cryst. 28 (2001) 351.
[41] M. Glogarova, Mol. Cryst. Liq. Cryst. 91 (1983) 309.
[42] A. Beresvev, V.G. Chigrinov, D.I. Dergachev, E.P. Poshidaev, J. Funfschilling, M. Schadt, Liq. Cryst. 5 (1989) 1171.
[43] N. Baytch, R.L.B. Selinger, J.V. Selinger, R. Shashidhar, Phys. Rev. E 68 (2003) 041702.
[44] J. Pavel, J. Phys. 45 (1984) 137.
[45] Ph. Martinot-Lagarde, Mol. Cryst. Liq. Cryst. 66 (1981) 61.
[46] R. Pindak, C.Y. Young, R.B. Meyer, N.A. Clark, Phys. Rev. Lett. 45 (1980) 1193.